

Study of simulated Bloch oscillations in strained graphene using neural networks.

J.A. González, C. E. López, A. Raya

Laboratorio de Inteligencia Artificial y Supercómputo
Instituto de Física y Matemáticas
Universidad Michoacana de San Nicolás de Hidalgo
Ciudad Universitaria. Edificio C-3
C.P. 58040
Morelia, Michoacán

August 2018

Abstract

We consider a monolayer of graphene under uniaxial, tensile strain and simulate Bloch oscillations for different electric field orientations parallel to the plane of the monolayer using several values of the components of the uniform strain tensor, but keeping the Poisson ratio in the range of observable values. We analyze the trajectories of the charge carriers with different initial conditions using an artificial neural network, trained to classify the simulated signals according to the strain applied to the membrane. When the electric field is oriented either along the Zig-Zag or the Armchair edges, our approach successfully classifies the independent component of the uniform strain tensor with up to 90% of accuracy and an error of $\pm 1\%$ in the predicted value. For an arbitrary orientation of the field, the classification is made over the strain tensor component and the Poisson ratio simultaneously, obtaining up to 97% of accuracy with an error that goes from $\pm 5\%$ to $\pm 10\%$ in the strain tensor component and an error from $\pm 12.5\%$ to $\pm 25\%$ in the Poisson ratio.

1 Introduction

Modern material science has received a tremendous impact after the first isolation of graphene membranes [1], giving rise to the era of 2D materials. Graphene possesses a number of outstanding properties, ranging from tremendously high electric and thermal conductivities, transparency of the membranes and, on top of that, stiffness and flexibility [2, 3, 4, 5]. Thus, the manipulation of electric properties through mechanical means has given rise to the field of straintronics [6] in graphene and other materials (see [7] for a recent review). On theoretical grounds, mechanical deformations of graphene membranes are usually accounted for through a strain tensor that describes the deviation of the graphene curvature with respect to the ideal flat case. The effect is then seen in tilting and displacing of the Dirac points in reciprocal space plus a re-shaping of these points such that the isoenergetic contours of these cones is elliptical, namely, the Fermi velocity becomes anisotropic and of tensor nature [7]. In the limiting case of uniform, tensile strain, these features might be completely understood as a strain modified reciprocal lattice such that the dispersion relation is modified from the pristine case by different constants (related to the components of the strain tensor) along the Armchair and Zig-Zag directions that in the low energy limit account for the anisotropy of the Fermi velocity [8, 9]. Considering this setup, in this article we explore the impact of strain in the scenario of Bloch oscillations (BO) in monolayer graphene.

BO are a remarkable phenomenon in traditional solid state physics. In spite of the fact that these oscillations are not directly observed in real solids, its study demonstrates the influence of a periodic array in conjunction with an external force field in the motion of charge carriers in different materials. The observation of BO has been done under several experimental settings in high-purity semiconductor superlattices [10, 11, 12, 13, 14, 15, 16, 17, 18, 19], atomic systems [20, 21], dielectric [22, 23, 24], plasmonic waveguide arrays [25] and also in bilayer graphene superlattices [26, 27]. All these observations make it relevant to study this phenomenon beyond solids. In this connection the inverse problem of BO has already been addressed by our group for the linear chain [28], the 2D square lattice [29] and pristine graphene [30] through an Artificial Neural Networks (ANN) approach. In this article we extend and generalize these findings to the case of graphene under uniaxial strain. As compared to the pristine case, the first natural difference that appears under strain is the change of the period of oscillations.

Moreover, it is observed that the amplitudes of closed trajectories change in such a way that new self-intersecting patterns appear [35]. Considering that machine learning methods are a consistent and reliable source to identify and classify patterns in general, we believe that a pointwise study of the modification of these oscillations by mechanical deformations of the membrane and its complete characterization using a specific setup of ANNs, is a natural question to be addressed.

ANN is part of the called machine learning methods, that actually are present in our daily life: the smartphones have facial, voice and fingerprint recognition, suggestion systems for the music and movies that we like, weather prediction, autonomous driving of vehicles and in many other applications. These machine learning methods learn to respond depending on the supplied data, where this data could represent information of practically any problem. For this reason they are used in several areas of science, in particular we have used the methods to analyze different physical systems, for example, gamma ray burst [31], obstruction detection inside pipes [32] and gravitational waves [33, 34] to mention some topics.

In this work we address the inverse problem of BO in uniaxially strained graphene under uniform extension of the membrane. We start in Section 2 by describing the dispersion relation of graphene under strain and the issue of BO at the semiclassical level. We further specify our considerations for the simulation of these BO in Section 3. The structure of the ANN is discussed in Section 4 and results presented in Section 5. We finally conclude in Section 6.

2 Bloch oscillations in strained graphene

We consider the connection between elasticity and the tight-binding description of graphene following closely reference [8]. Considering the honeycomb array of graphene as the superposition of two triangular sublattices, the position of the atoms in the deformed sublattice A (see Fig. 1) can be written as $\mathbf{x}' = (I + \epsilon)\mathbf{x}$, where I is the identity matrix and ϵ is the coordinate independent strain tensor. Thus, the nearest-neighbor tight-binding Hamiltonian is expressed as

$$H = - \sum_{\mathbf{x}', n} t_n a_{\mathbf{x}'}^\dagger b_{\mathbf{x}' + \boldsymbol{\delta}'_n} + h.c., \quad (1)$$

where \mathbf{x}' runs over all the grid points of the sublattice A and $\boldsymbol{\delta}'_n$ are the vectors connecting every point with the nearest neighbors. Here, $a_{\mathbf{x}'}^\dagger$ and

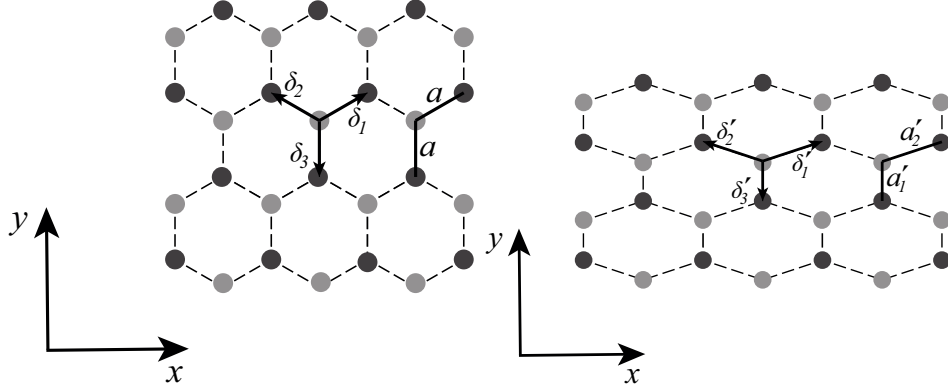


Figure 1: Crystal structure of graphene. *Left panel:* Pristine case. *Right panel:* Under uniaxial, tensile strain.

$b_{\mathbf{x}'+\delta'_n}$ are the creation and annihilation operators for charge carriers in the sublattices A and B respectively at the corresponding sites \mathbf{x}' and $\mathbf{x}' + \delta'_n$. Notice that the hopping parameters t_n in the Hamiltonian (1) are considered coordinate independent, assumption that is valid only for the case of uniform strain. Upon Fourier expanding the creation and annihilation operators, in momentum space, the tight-binding Hamiltonian has a form very similar to the ideal case, namely,

$$H = - \sum_{\mathbf{k}, n} t_n e^{-i\mathbf{k} \cdot (I+\epsilon) \cdot \delta_n} a_{\mathbf{k}}^\dagger b_{\mathbf{h}} + h.c., \quad (2)$$

with the difference that the hopping parameters are now position-dependent. The dispersion relation is straightforwardly obtained as

$$\varepsilon(\mathbf{k}) = \pm \left| \sum_n t_n e^{-i\mathbf{k}^* \cdot \delta_n} \right|, \quad (3)$$

with $\mathbf{k}^* = (I + \epsilon) \cdot \mathbf{k}$. At the linear order on the strain tensor, we write

$$t_n = t_0 \left(1 - \frac{\beta}{a^2} \boldsymbol{\delta}_n \cdot \boldsymbol{\epsilon} \right) \boldsymbol{\delta}_n, \quad (4)$$

where t_0 is the hopping parameter of pristine graphene and $\beta \simeq 3$ is the variation of the hopping energy due to lattice deformation. Then, using that

$$\boldsymbol{\delta}_1 = \frac{a}{2}(\sqrt{3}, 1), \quad \boldsymbol{\delta}_2 = \frac{a}{2}(-\sqrt{3}, 1), \quad \boldsymbol{\delta}_3 = a(0, -1), \quad (5)$$

with a the interatomic distance in an ideal sample, we explicitly have

$$\varepsilon(\mathbf{k}) = \pm t_0 \sqrt{3 + f(\mathbf{k}^*) - \beta(3\text{Tr}(\epsilon) + f_\epsilon(\mathbf{k}^*) + \beta^2 f_{\epsilon^2}(\mathbf{k}^*))}, \quad (6)$$

where

$$f(\mathbf{k}^*) = 2 \cos\left(\sqrt{3}k_x^* a\right) + 4 \cos\left(\frac{\sqrt{3}k_x^* a}{2}\right) \cos\left(\frac{3k_y^* a}{2}\right), \quad (7)$$

whereas $f_\epsilon(\mathbf{k}^*)$ and $f_{\epsilon^2}(\mathbf{k}^*)$ represent modifications of the spectrum at first and second order in β , respectively. For the analysis in this paper, we consider $\beta = 0$ and use the simplified dispersion relation

$$\varepsilon(\mathbf{k}) = \pm t_0 \sqrt{3 + f(\mathbf{k}^*)} \quad (8)$$

and leave the full dispersion relation for a future work.

For the analysis of BO, we consider the semiclassical equation of motion

$$\frac{d\mathbf{k}}{dt} = -e\mathbf{E}, \quad (9)$$

where \mathbf{E} represents a static, uniform electric field and e is the fundamental charge. After integration, we obtain the expression $\mathbf{k}(t) = \mathbf{k}(0) - e\mathbf{E}t$ and we substitute it into the dispersion relation (8)

$$\frac{d\mathbf{r}}{dt} = \frac{\partial \varepsilon(\mathbf{k})}{\partial \mathbf{k}}. \quad (10)$$

Integrating this equation we can obtain the position of the charge carriers at a given time t . We consider a strain tensor of the form

$$\epsilon = \begin{pmatrix} \epsilon_{xx} & 0 \\ 0 & -\nu\epsilon_{xx} \end{pmatrix}, \quad (11)$$

with the Poisson ratio ν . Below we detail the procedure to simulate BO in strained graphene from this framework.

3 Simulated Bloch oscillations

Once we have the equations that describe the position of the electric charge carriers as a function of time, we need to specify some initial conditions like the initial momentum $(k_x(0), k_y(0))$ or the external electric field (E_x, E_y)

and simulate the trajectories of the carriers for a fixed lapse, only varying the strain. Additionally we consider that $\hbar = a = \tau = 1$ and $e = -1$ for a time interval of $T = 4\pi$ units. Notice that with these assumptions, the analyzed quantities do not have physical units.

Two cases are studied according to the parameters that are varied when the oscillations are generated numerically:

1. The only parameter that varies is ϵ_{xx} with $\epsilon_{xy} = \epsilon_{yx} = 0$, $\nu = 0.16$ and the other parameters fixed in three subcases
 - a) $E_x = 1$, $E_y = 0$, $k_x(0) = 0$, $k_y(0) = \pi/\sqrt{3}$.
 - b) $E_x = 0$, $E_y = 1$, $k_x(0) = \pi/\sqrt{3}$, $k_y(0) = 0$.
 - c) $E_x \neq 0$, $E_y \neq 0$, $k_x(0) = k_y(0) = 0$.
2. The parameters that vary are ϵ_{xx} and ν with $E_x \neq 0$, $E_y \neq 0$, $k_x(0) = k_y(0) = 0$ and $\epsilon_{xy} = \epsilon_{yx} = 0$.

In the first case, N different values are used for ϵ_{xx} and they are equidistant in the interval $[0, 0.25]$ and labeled in C_ϵ classes or groups, such that each class has the same number of simulations, *i.e.* $\text{mod}(N/C_\epsilon) = 0$ must be satisfied. The ANN will perform a classification using as input data for training, the components $x(t)$ and $y(t)$ of the electric carrier position. We interpret each predicted class as a value for ϵ_{xx} with a relative error related with the total length of the interval $\epsilon_L = 0.25$. We define

$$\hat{\epsilon}_m = (2m - 1)\epsilon_L/2C_\epsilon \pm \epsilon_L/2C_\epsilon, \quad 1 \leq m \leq C_\epsilon, \quad (12)$$

as the predicted value of ϵ_{xx} associated with the class m , where C_ϵ is the total number of classes.

The second case is similar to the first one, but now also the parameter ν is varied in the interval $[0, 0.2]$ selecting N' different equidistant values and grouping them in C_ν classes. In this scenario the total number of generated patterns is $N \times N'$ and the ANN classifies both of the parameters simultaneously: ϵ_{xx} is associated to one class from the total of C_ϵ and ν to one class from C_ν classes. The predicted value for ν has a similar expression as in Eq. (12)

$$\hat{\nu}_n = (2n - 1)\nu_L/2C_\nu \pm \nu_L/2C_\nu, \quad 1 \leq n \leq C_\nu, \quad (13)$$

with $\nu_L = 0.2$ the total length of the interval where ν is varied.

In Eqs. (12) and (13) we observe that as we increase the number of classes, the error associated with each prediction is smaller. It is worth to mention that as the errors in the predictions decrease, also the efficiency in the classification decreases, as we will illustrate in the next section. This numerical approach, where simulations are generated and classifications are studied considering different values for the parameters and the number of classes, was previously used in [28, 29, 30] where are studied Bloch oscillations in simpler physical systems.

4 Artificial neural networks

We use a feedforward ANN to classify patterns such that the network estimates the parameters ϵ and ν that generated the numerical simulations. To train the ANN first it is required to preprocess the data that will feed into the network. Also, as we are working with a supervised learning algorithm, we have to define the targets associated with each one of the patterns.

The input data used, is obtained from two time series: the position $x(t)$ and $y(t)$ of the charge in a simulated BO in the time interval $0 \leq t \leq T$ (where T is the total duration of the oscillation), subject to different imposed conditions and the position is obtained integrating numerically the Eq. (10). We have divided the simulation in fifty steps in time such that $t_i = i\Delta t$, with $0 \leq i \leq 49$ and $\Delta t = T/50$. The input vector for each pattern p is constructed as

$$I^p = \{x(t_0), y(t_0), \dots, x(t_{49}), y(t_{49})\}, \quad 1 \leq p \leq N_p, \quad (14)$$

with N_p the total number of patterns. As mention in the previous section, $N_p = N$ in the first case and $N_p = N \times N'$ in the second. From the total number of patterns, seventy percent of them are chosen randomly to train the network and the remaining thirty percent corresponds to the validation set. The purpose of this validation set is to avoid that the training process reaches a state of overtraining, producing an excellent behavior during the prediction of the training set, but having a bad performance over patterns not used in the training. To test the performance of the network, the same number of signals as in the validation set are simulated but this time using

random values of the variables ϵ_{xx} and ν , ensuring that the new simulations are inside the range under consideration. The selection of the training and validation sets is made once that the target values for the patterns have been prepared.

The activation functions used in the hidden and output layers are sigmoid functions. These are chosen such that the output values are in the open interval (0,1). Then, we define the target values for C_ϵ and C_ν , representing the different classes in the range of the function. The proposed targets associated with each pattern and class are:

$$\begin{aligned}\hat{T}_{\epsilon_m} &= (2m - 1)/(2C_\epsilon), \quad 1 \leq m \leq C_\epsilon, \\ \hat{T}_{\nu_n} &= (2n - 1)/(2C_\nu), \quad 1 \leq n \leq C_\nu,\end{aligned}\tag{15}$$

where \hat{T}_{ϵ_m} is the target for all the patterns that are in the class m and \hat{T}_{ν_n} is the target for all the patterns that are in the class n . For example, if the ANN is fed with one pattern among the first N/C_ϵ it will be part of the class $m = 1$ and the corresponding target is $\hat{T}_{\epsilon_1} = 1/2C_\epsilon$.

The ANN was programmed in FORTRAN 90 and trained with an offline supervised backpropagation learning algorithm designed to minimize a cost function type mean squared error [36, 37]. The generation of the simulated BOs, the preprocessing of the data and also the visualization of the results was performed with Wolfram Mathematica.

The structure of the network has one input layer with two hundred neurons that receive the extracted data from each pattern, one hidden layer with a variable number of neurons to be determined according to ANN performance and one output layer with one neuron in the first case, and two neurons in the second case. One of the output neurons produce a value that is related to ϵ_{xx} and the other to ν . For this reason the structure of the output layer changes depending on the case.

With the input data, the desired outputs and the network structure ready, it is necessary to train the network for a suitable number of iterations and evaluate the performance of ANN counting the number of predictions correctly classified. We consider that the pattern has been correctly classified if the output of the network corresponding to this pattern has an output value between $\hat{T}_{\epsilon_m} - 1/2C_\epsilon$ and $\hat{T}_{\epsilon_m} + 1/2C_\epsilon$. A similar condition is employed to define a correct classification when the output corresponding to the variable

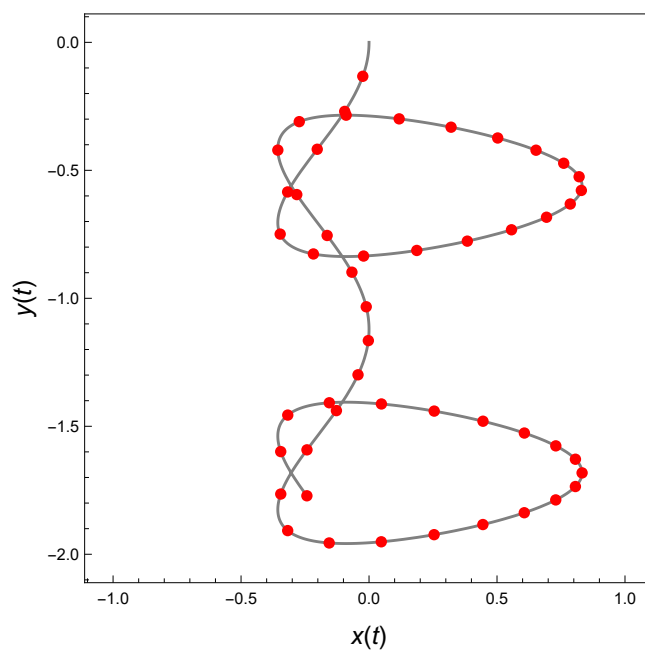


Figure 3: Sample of the trajectory of an electron when $\epsilon_{xx} = 0.20$ during the time interval $0 \leq t \leq 4\pi$ and the initial conditions considered for the case 1b. The red dots represent the coordinates used as inputs for the ANN.

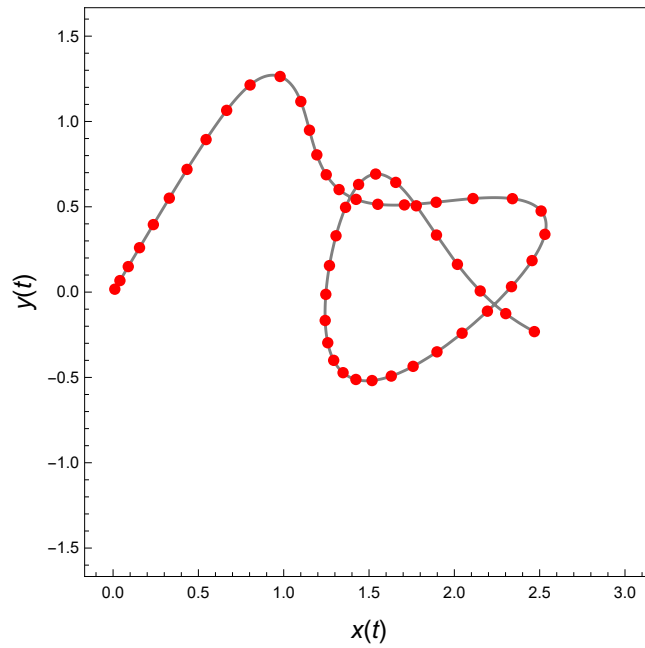


Figure 4: Sample of the trajectory of an electron when $E_x = -0.33$, $E_y = -0.79$ and $\epsilon_{xx} = 0.20$ during the time interval $0 \leq t \leq 4\pi$ and the initial conditions considered for the case 1c. The red dots represent the coordinates used as inputs for the ANN.

Once we have selected the network with the parameters that produces the lowest cost during training, the network performance is evaluated calculating the Percentage of Predictions Correctly Classified (PPCC) in each case and the results are displayed in Table 1. We can observe that for each of the subcases, the more considered classes, the lower the PPCC as it is expected. We also observe, in one hand that the best performance is obtained in case 1a), and in the other the case 1c) (where both components of the electric field are different from zero) it has the lower PPCC. As mentioned before, although the PPCC is lower when the number of classes increases, the error associated to the predicted average value is lower as established Eq. (12). Hence the error associated with the average value $\hat{\epsilon}$ is of $\pm 1\%$ of ϵ_L when the simulations are divided in fifty classes, meanwhile the error associated is of $\pm 0.25\%$ of ϵ_L when two hundred classes are selected. Depending on the accuracy needed, we can chose the number of classes in which the patterns are divided.

Case 1a			
PPCC(%) for	Training	Validation	Test
$C_\epsilon = 50$	90.1	90.0	88.6
$C_\epsilon = 100$	82.5	77.6	86.0
$C_\epsilon = 200$	82.1	77.0	79.0
Case 1b			
$C_\epsilon = 50$	88.1	86.6	90.3
$C_\epsilon = 100$	80.2	75.6	79.6
$C_\epsilon = 200$	68.4	65.0	68.3
Case 1c			
$C_\epsilon = 50$	81.8	86.6	81.6
$C_\epsilon = 100$	66.7	65.3	69.0
$C_\epsilon = 200$	59.5	52.6	54.6

Table 1: PPCC obtained by the ANN for the training, validation and test sets in case 1. The output generated by the network predicts the value of ϵ_{xx} .

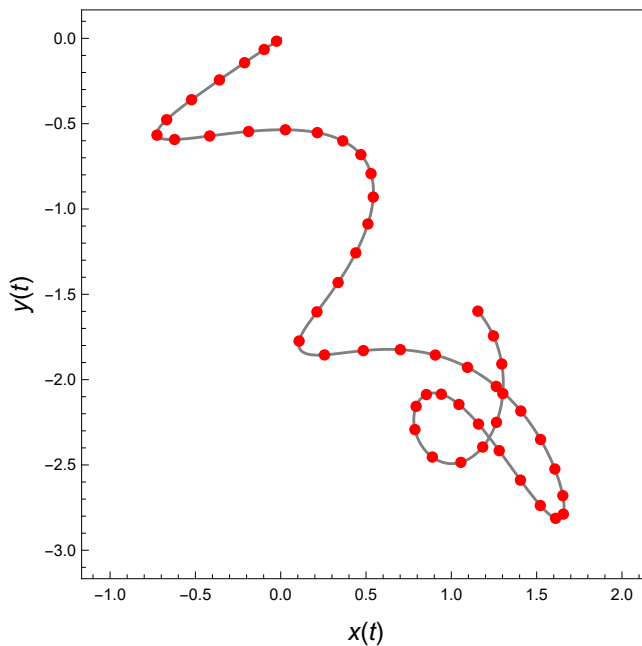


Figure 5: Sample of the trajectory of an electron when $E_x = 0.76$, $E_y = 0.78$, $\epsilon_{xx} = 0.20$, and $\nu = 0.16$ during the time interval $0 \leq t \leq 4\pi$ and the initial conditions considered for the case two. The red dots represent the coordinates used as inputs for the ANN.

5.2 Prediction of ϵ_{xx} and ν

For the second case of study we created the same amount of simulations as in the previous case but selecting $N = 50$ and $N' = 20$, varying ϵ_{xx} and ν respectively and considering $C_\epsilon = 5$ and 10 classes for ϵ_{xx} and $C_\nu = 2$ and 4 classes for ν . E_x and E_y were selected randomly in the interval $[-1,1]$, showing a sample of the trajectory for the considered lapse of time and initial conditions in Fig. (5).

The PPCC for this case are shown in the Table 2.

The behavior of the PPCC is similar to case 1, obtaining more correctly classified patterns when less classes are considered. As the number of simulations is the same as in the previous case, but with two parameters that vary, the total number of classes for each parameter is less. As a consequence, the associated errors for the predicted value of ϵ_{xx} are $\pm 5\%$ and $\pm 10\%$ of ϵ_L for 10 and 5 classes respectively and an error for the predicted value of ν of

Case 2				
PPCC(%) for	Output	Training	Validation	Test
$C_\epsilon = 5$	O_1	99.8	100.0	96.3
$C_\nu = 2$	O_2	99.0	98.0	97.3
$C_\epsilon = 5$	O_1	99.4	98.0	97.6
$C_\nu = 4$	O_2	91.4	91.3	88.3
$C_\epsilon = 10$	O_1	95.1	96.0	92.6
$C_\nu = 2$	O_2	92.7	92.1	94.0
$C_\epsilon = 10$	O_1	98.5	98.0	84.3
$C_\nu = 4$	O_2	83.1	83.6	87.0

Table 2: PPCC obtained by the ANN for the training, validation and test sets in case 2. The output O_1 predicts the value of ϵ_{xx} and the output O_2 the one of ν . Both predictions were divided in C_ϵ and C_ν classes respectively.

$\pm 12.5\%$ and $\pm 25\%$ of ν_L for 4 and 2 classes respectively.

6 Conclusions

In this work we have considered the inverse problem of BO in strained graphene. We have considered the situation of uniaxially, uniform, tensile strain described by a diagonal, coordinate independent strain tensor in the corresponding tight-binding description of graphene. From the resulting dispersion relation, in the limit when the variation of the hopping energy due to the displacement of carbon atoms vanishes, such that the said dispersion relation is described in Eq. (8), within a semiclassical approximation, we simulate BO for different electric field orientations and varying the Poisson ratio, keeping the rest of the parameters of the model fixed. Feeding the ANN with 700 training signals, we were able to classify the components of the strain tensor for 300 new randomly generated signals.

For the case 1, when the component E_y of the external electric field applied to the graphene is zero, the network has an accuracy in their predictions for ϵ_{xx} that goes from 79.0% to 88.6% with an error of $\pm 0.25\%$ and $\pm 1\%$ respectively.

Analogously, when $E_x = 0$ the network has an accuracy in their predictions

for ϵ_{xx} that goes from 68.3% to 90.3% with an error of $\pm 0.25\%$ and $\pm 1\%$ respectively.

When the external electric field has a random orientation, the accuracy predicting ϵ_{xx} goes from 54.6% to 81.6% with an error of $\pm 0.25\%$ and $\pm 1\%$ respectively.

In the case 2, the network predict simultaneously ϵ_{xx} and ν for a random electric field orientation, obtaining an accuracy of 96.3% with an error of $\pm 10\%$ predicting ϵ_{xx} and an accuracy of 97.3% with an error of $\pm 25\%$ predicting ν . This situation has the higher accuracy but also the higher error associated to each parameter. For the scenario with the lower error associated, the network has an accuracy of 84.3% with an error of $\pm 5\%$ predicting ϵ_{xx} and an accuracy of 87.0% with an error of $\pm 12.5\%$ predicting ν . These results can be improved increasing the number of simulations that feed the ANN, but also increasing the computational time used during the network's training.

These encouraging results motivate us to pursue a more complete study of the full dispersion relation (6) [35]. This is work in progress and results will be presented elsewhere.

7 Acknowledgments

The authors would like to thank Saul Hernández-Ortiz for very useful discussions. We acknowledge support from Consejo Nacional de Ciencia y Tecnología (México) under grant 256494 and CIC-UMSNH under grant 4.23. We also thank for providing computer resources to ABACUS Laboratorio de Matemáticas Aplicadas y Cómputo de Alto Rendimiento del CINVESTAV-IPN under grant CONACT-EDOMEX-2011-C01-165873.

References

- [1] Novoselov K S, Geim A K, Morozov S V, Jiang D, Zhang Y, Dubonos S V, Grigorieva I V and Firsov A A 2004, *Science* **306**, 666.
- [2] Novoselov K S, McCann E, Morozov S V, Falko V I, Katsnelson M I, Zeitler U, Jiang D, Schedin F and Geim A K 2006, *Nat. Phys.* **2**, 177.

- [3] Katsnelson M I 2007, *Materials Today* **10**, 20.
- [4] Novoselov K S, Jiang Z, Zhang Y, Morozov S V, Stormer H L, Zeitler U, Maan J C, Boebinger G S, Kim P and Geim A K, *Science* **315**, 1379.
- [5] Geim A K and Novoselov K S 2007, *Nat. Mater.* **6**, 183.
- [6] Pereira V M, Castro Neto A H and Peres N M R 2009, *Phys. Rev. B* **80**, 045401.
- [7] García-Naumis G, Barraza-Lopez S, Oliva-Leyva M and Terrones H 2017, *Rep. Prog. Phys.* **80**, 096501.
- [8] Oliva-Leyva M and García-Naumis G 2013, *Phys. Rev. B* **88**, 085430.
- [9] Concha Y, Huet A, Raya A and Valenzuela D 2018, *Mater. Res. Express* **5**, 065607.
- [10] J. Feldmann, K. Leo, J. Shah, D.A.B. Miller, J.E. Cunningham, T. Meier, G. von Plessen, A. Schulze, P. Thomas, S. Schmitt-Rink, *Phys. Rev. B* 46 (1992) 7252.
- [11] G. von Plessen, P. Thomas, *Phys. Rev. B* 45 (1992) 9185.
- [12] K. Leo, P.H. Bolivar, F. Brüggemann, R. Schwedler, K. Köhler, *Solid State Commun.* 84 (1992) 943.
- [13] P. Leisching, P. Haring Bolivar, W. Beck, Y. Dhaibi, F. Brüggemann, R. Schwedler, H. Kurz, K. Leo, K. Köhler, *Phys. Rev. B* 50 (1994) 14389.
- [14] T. Dekorsy, P. Leisching, K. Köhler, H. Kurz, *Phys. Rev. B* 50 (1994) 8106.
- [15] T. Dekorsy, R. Ott, H. Kurz, K. Köhler, *Phys. Rev. B* 51 (1995) 17275.
- [16] C. Waschke, H.G. Roskos, R. Schwedler, K. Leo, H. Kurz, K. Köhler, *Phys. Rev. Lett.* 70 (1993) 3319.
- [17] H.G. Roskos, C. Waschke, R. Schwedler, P. Leisching, Y. Dhaibi, H. Kurz, K. Köhler, *Superlattices Microstruct.* 15 (1994) 281.
- [18] A.R. Kolovsky, H.J. Korsch, *Phys. Rev. A* 67 (2003) 063601.

- [19] D. Witthaut, F. Keck, H.J. Korsch, S. Mossmann, *New J. Phys.* **6** (2004) 41.
- [20] M.B. Dahan, E. Peik, J. Reichel, Y. Castin, C. Salomon, *Phys. Rev. Lett.* **76** (1996) 4508–4511.
- [21] M. Genske, *et al.*, *Phys. Rev. Lett.* **110** (2013) 190601.
- [22] T. Pertsch, P. Dannberg, W. Elflein, A. Bräuer, F. Lederer, *Phys. Rev. Lett.* **83** (1999) 4752.
- [23] R. Morandotti, U. Peschel, J.S. Aitchison, H.S. Eisenberg, Y. Silberberg, *Phys. Rev. Lett.* **83** (1999) 4756–4759.
- [24] R. Sapienza, *et al.*, *Phys. Rev. Lett.* **91** (2003) 263902.
- [25] A. Block, *et al.*, *Nat. Commun.* (2014) 53843.
- [26] Hemeng Cheng, *et al.*, *Appl. Phys. Lett.* **105** (2014) 072103.
- [27] Changan Li, *et al.*, *Appl. Phys. Lett.* **103** (2013).
- [28] J. A. González, C. E. López, S. Hernández-Ortiz and A. Raya, *Plasmonics* **13**, 9 (2016).
- [29] M. Carrillo, J. A. González, S. Hernández-Ortiz, C.E. López and A. Raya *Com. Mat. Sci.* **137**, 1 (2017).
- [30] M. Carrillo, J. A. González, S. Hernández-Ortiz, C. E. López and A. Raya, *Comp. Cond. Mat.* **13**, 104 (2017).
- [31] F. Rivera-Paleo, C. E. López, F.S. Guzmán, J. A. González, *Phys. Rev. D*, **95**, pp. 1-9, (2017).
- [32] M. Carrillo, J. A. González, C. E. López and U. Que, *Phys. Rev. E*, **96**, pp. 1-10, (2017).
- [33] M. Carrillo, M. Gracia-Linares, J. A. González, F. S. Guzmán *Gen. Rel. Grav.*, **48**, no. 10, 141, (2016).
- [34] M. Carrillo, M. Gracia-Linares, J. A. González, F. S. Guzmán *International Journal of Modern Physics D*, **27**, 1850043, (2018).

- [35] S. Hernández-Ortiz et al., work in progress.
- [36] R. Rojas, Springer-Verlag, (1996).
- [37] C. M. Bishop, Springer, (2006).